Electronic Supplementary Material (ESI) for Physical Chemistry Chemical Physics.

Electronic Supplementary Information for Prediction Model for Nanoparticle Diffusion Behavior in Fibrous Materials Considering Steric and Hydrodynamic Resistances

D. Tian [a], Z.G. Qu [a], T. Lai [a], G.D. Zhu [b]*

E-mail address: zgqu@mail.xjtu.edu.cn (Z.G. Qu).

[a]MOE Key Laboratory of Thermal-Fluid Science and Engineering,

School of Energy and Power Engineering,

Xi'an Jiaotong University,

Xi'an 710049, China

[b]Department of Urology,

The First Affiliated Hospital of Xi'an Jiaotong University,

Xi'an, 710061, China.

Table of contents

S1. Simulation section

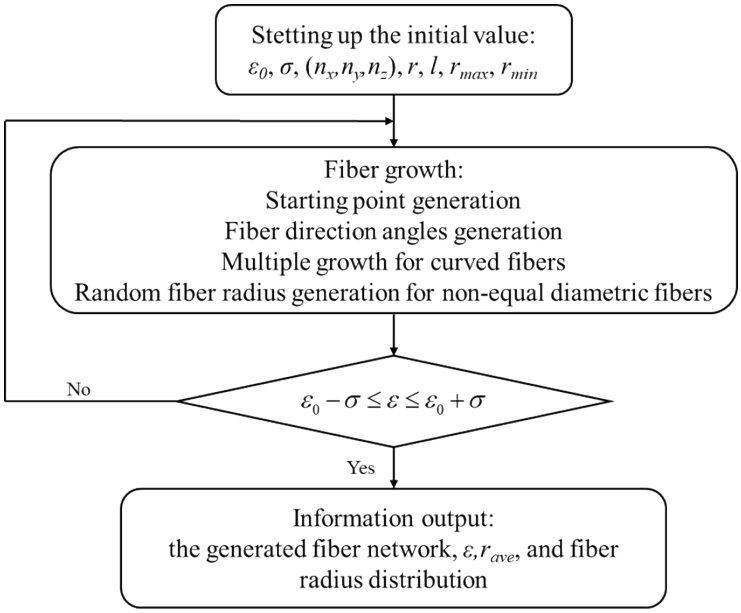

Fig. S1. Flow diagram of fiber networks reconstruction

Table S1. Parameters of fiber networks reconstruction

Parameter symbol	Physical significance	Value range
$\varepsilon_{0,}\varepsilon$	expected and output porosity	0.15-0.99
σ	porosity deviation	0.002
$n_x \times n_y \times n_z$	grid resolution	100×100×100 (lattices)
r_f	fiber radius	1-6 lattices
l	curvature of fibers	1, 3, 5
r_{max}, r_{min}	maximum and minimum fiber radius	1 and 5 lattices

Figure S2 shows the three types of fiber networks reconstructed based on the above reconstruction method. The porosity is the same for three fibrous structures (i.e., $\varepsilon = 0.8$). Figure S2(a) displays a fibrous structure with isodiametric straight fibers, the fiber orientation is random. Figure S2(b) displays a fibrous structure with isodiametric curved fibers, the curvature of fibers is 3 (1/lattice). Figure S2(c) displays a fibrous structure with non-equant straight fibers. Figure S2(d) shows the fiber radius distribution of non-equant straight fibers, the fiber radius is randomly distributed in the range from 1 to 5 lattices and the dotted line is shown as the average fiber radius of a non-equant fiber network.

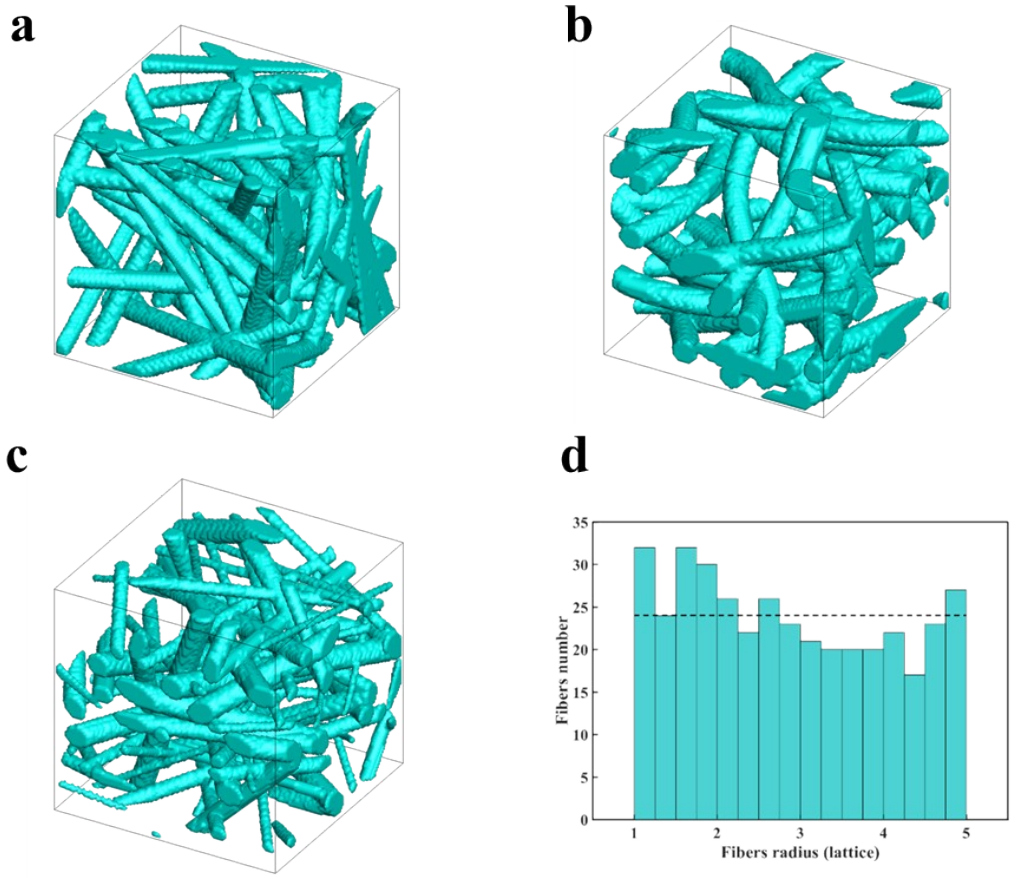

Fig. S2. Reconstructed fibrous porous medium and fibers radius distribution. (a) Isodiametric straight fibers ($\varepsilon = 0.8; r = 4$). (b) Isodiametric curved fibers. ($\varepsilon = 0.8; r = 4; l = 3$). (c) Non-equant straight fibers ($\varepsilon = 0.8; r_{\min} = 1; r_{\max} = 5$). (d) Non-equant straight fibers radius distribution.

S1.1 Physical model

To obtain the accuracy and universal combined model, the accurate steric and hydrodynamic resistance model is required to be firstly presented. The steric and hydrodynamic resistance of nanoparticle diffusion are calculated respectively based on random reconstruction. The physical model is shown in Figure S3. For steric resistance, the long-range hindered Brownian motion of a large number of particles in fibrous media is simulated. It is assumed that the position of particles and fibers are not overlapped and the interactions between particles are not considered. For hydrodynamic resistance, permeability is the link of structure parameters and hydrodynamic resistance. The seepage in the porous medium is simulated to determine the constitutive relation between the structural parameters and permeability. The flow is assumed to be incompressible laminar flow. Table 3 present the parameters of the physical model. The steric and hydrodynamic resistance are calculated in the domain with the same size: $l_x \times l_y \times l_z$, where l_x, l_y, and l_z are the domain lengths along with the x, y, and z directions, respectively. The fiber radius is defined as r_f, and the nanoparticle radius is defined as r_s. The fiber and solute are both assumed to be rigid and undeformable.

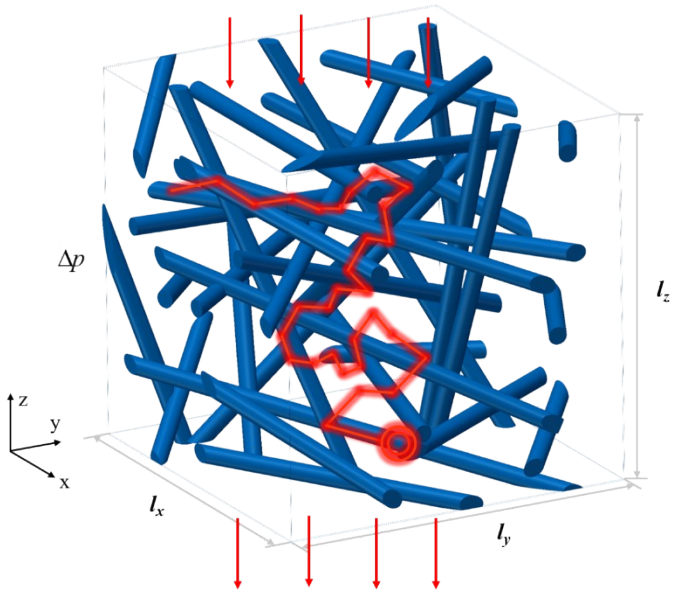

Fig. S3. Schematic of the physical model

Table S2. Parameters of the physical model

Parameter symbol	Physical significance	Value range
$l_x \times l_y \times l_z$	simulation domain size	30 μm x 30 μm x 30 μm
N	simulated nanoparticle number	10^5
r_f	fiber radius	0.3-1.8 μm
r_s	nanoparticle radius	10-50 nm
Δp	pressure gradient	57.6Pa

S1.2 Steric resistance

Fig. S4 presented the time-evolution of dimensionless effective diffusivity D_{ste}/D_0. As the determination of the long-range or short-range diffusion, the diffusive time is defined as a dimensionless time shown as follow:

$$t^* = 6D_0/l_x^2 \tag{S4}$$

As shown in Fig. S4, the nanoparticle diffusion in the fibrous media is close to the free diffusion ($D_{ste}/D_0 \approx 1$) when the diffusive time $t^* \le 0.5$. Therefore, long-range simulation ($t^* \ge 2$) was used to obtain the diffusion coefficient in the present work for avoiding the fluctuation of diffusion coefficient caused by short-range diffusion.

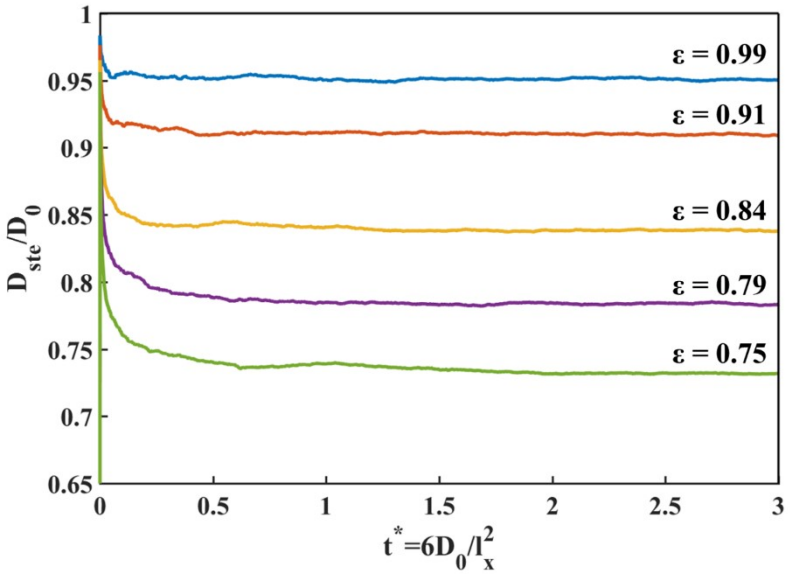

Fig. S4. Time-evolution of the normalized diffusion coefficient for selected porous media at different porosity.

To validate the method of the simulation, the independence of parameters (tracer number and unit time step) and effective diffusivity are tested. In a range of N ($10^5 \le N \le 10^7$) and Δt ($1.47ns \le \Delta t \le 14.7ns$), the change of effective diffusivity is less than 0.5%. Further, to verify the availability of the present numerical method for porous media, the nanoparticle

diffusion process in periodically packed spheres was simulated and compared with the analytical approach[1]. The spheres are periodically packed at the face center and apex angle of the cubic with a uniform diameter. The solid sphere forms the porous skeleton, and the remaining area not occupied by the sphere is pore space. By changing the sphere diameter, the ordered porous media with different porosity is obtained.

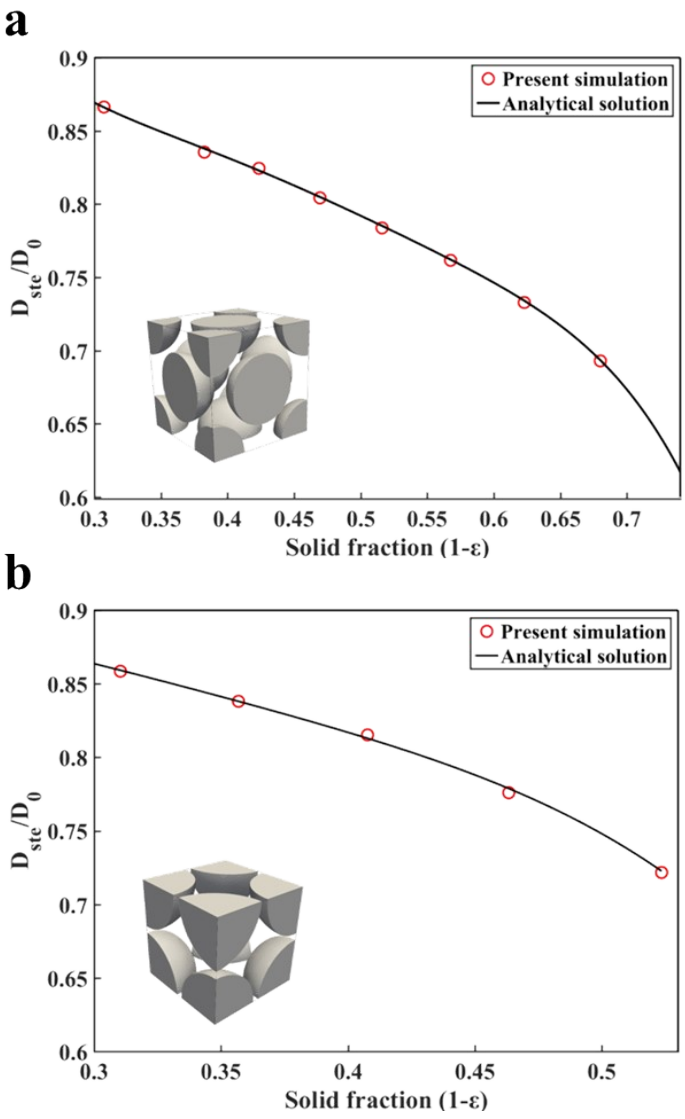

Fig. S5. Normalized diffusion coefficient D_{eff}/D_0 in FCC (a) and SC (b) sphere arrays, obtained from the analytical solution[1] (solid circles), with RW simulation (open circles)

S1.3 Hydrodynamic resistance

To validate the accuracy of seepage simulation, the independence of the pressure gradient and permeability should be tested first. Under the premise of laminar flow, a range of pressure gradients $5.76Pa \le \Delta p \le 576Pa$ is simulated, and the change in permeability is less than 1%. Furthermore, the creeping flow in regular parallel fibers is simulated to validate the method of fibrous media flow.

Fig. S6 displays a schematic diagram of the computing domain with periodic boundary conditions on both sides. The fibers are arranged in an infinite hexagonal array. The grid number of the computing domain is $\sqrt{3}h \times h \times 1$. The radius of the fiber is fixed, and the value of *h* is changed to achieve different porosities. Since the fiber remains constant in the direction of height, the three-dimensional simulation is realized by setting the periodic boundary conditions and 1 lattice height. As shown in Fig. S4, the simulated results are compared with the analytical solution presented by Gebart et al.[2] and the SRT-LBM results simulated by Nabovati et al. [3] The analytical solution is shown as follows:

$$\frac{K}{r_f^2} = C\left(\sqrt{\frac{1-\phi_c}{1-\varepsilon}} - 1\right)^b \tag{S2}$$

where ϕ_c is the percolation threshold, and *b* and *C* are geometric factors. When the fiber arrays are hexagonal, ϕ_c is $1-\pi/4$, *C* is $16/9\sqrt{2}\pi$, and *b* is 2.5. Over the range of porosity from 0.15 to 0.6, both simulated results have excellent agreement with the analytical solution. However, it is noteworthy that the fit between the present MRT model and the analytical solution is better than the fit of the SRT model in the porosity range of 0.7-0.9. This finding

further demonstrates the capability of the present numerical method in simulating fluid flow in fibrous porous media for a large range of porosities.

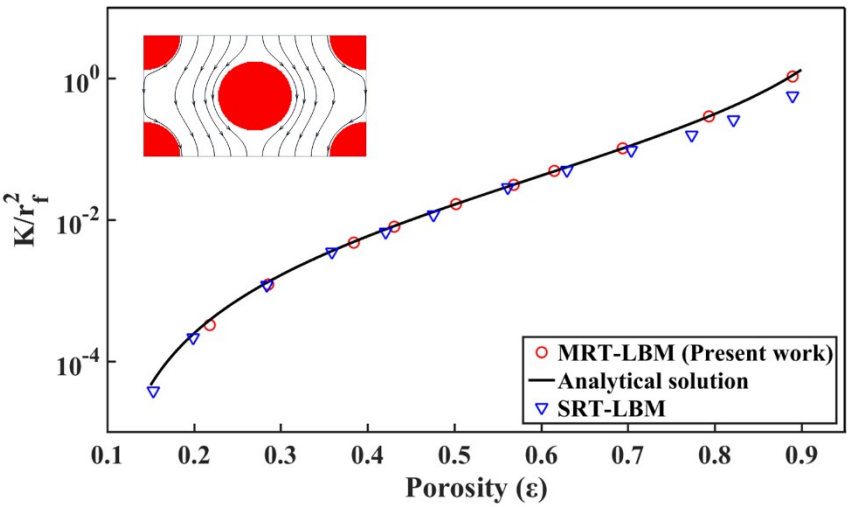

Fig. S6. Normalized permeability of the parallel fibrous media is plotted from the analytical solution (line), with MRT-LBM (circles) and SRT-LBM (inverted triangles)

S1.4 Applicability of the dual-resistance model in curved fiber and random distribution radius fiber

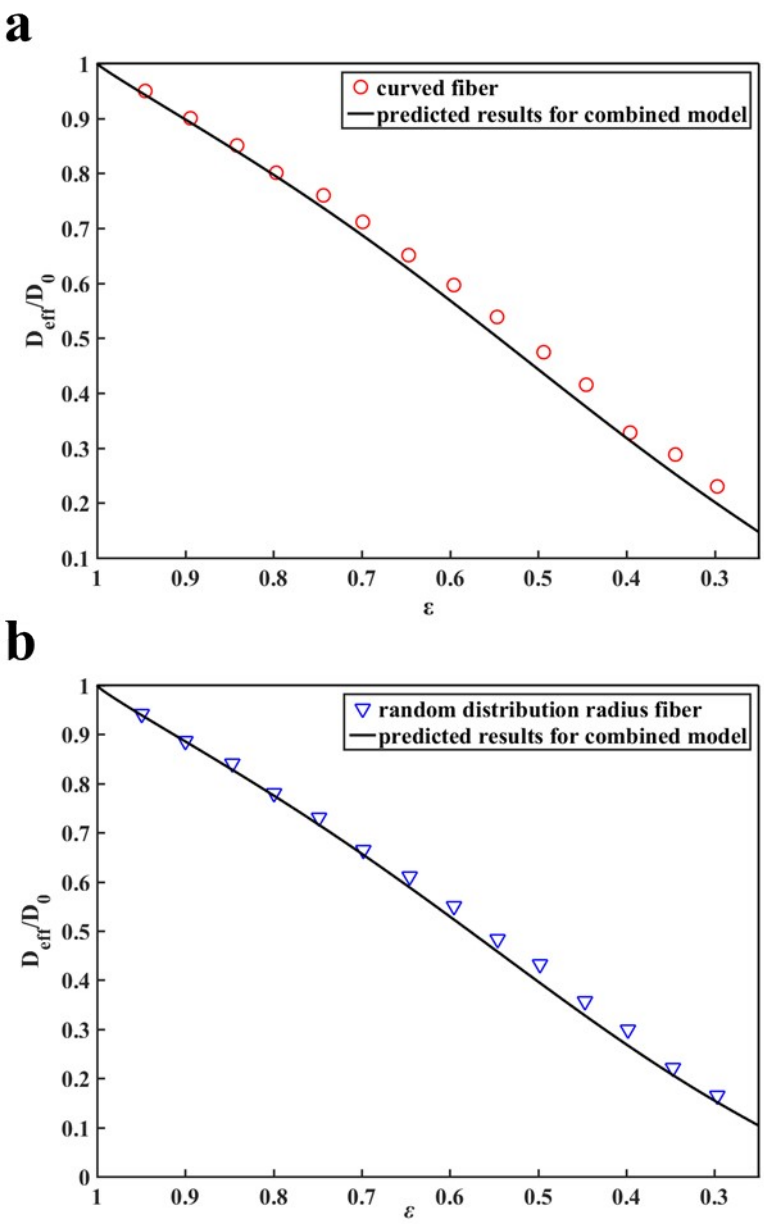

Fig. S7 Effect of fiber structure on nanoparticle diffusion (a) Randomly curved fibers (b) random distribution radius fibers

S2 Experimental section

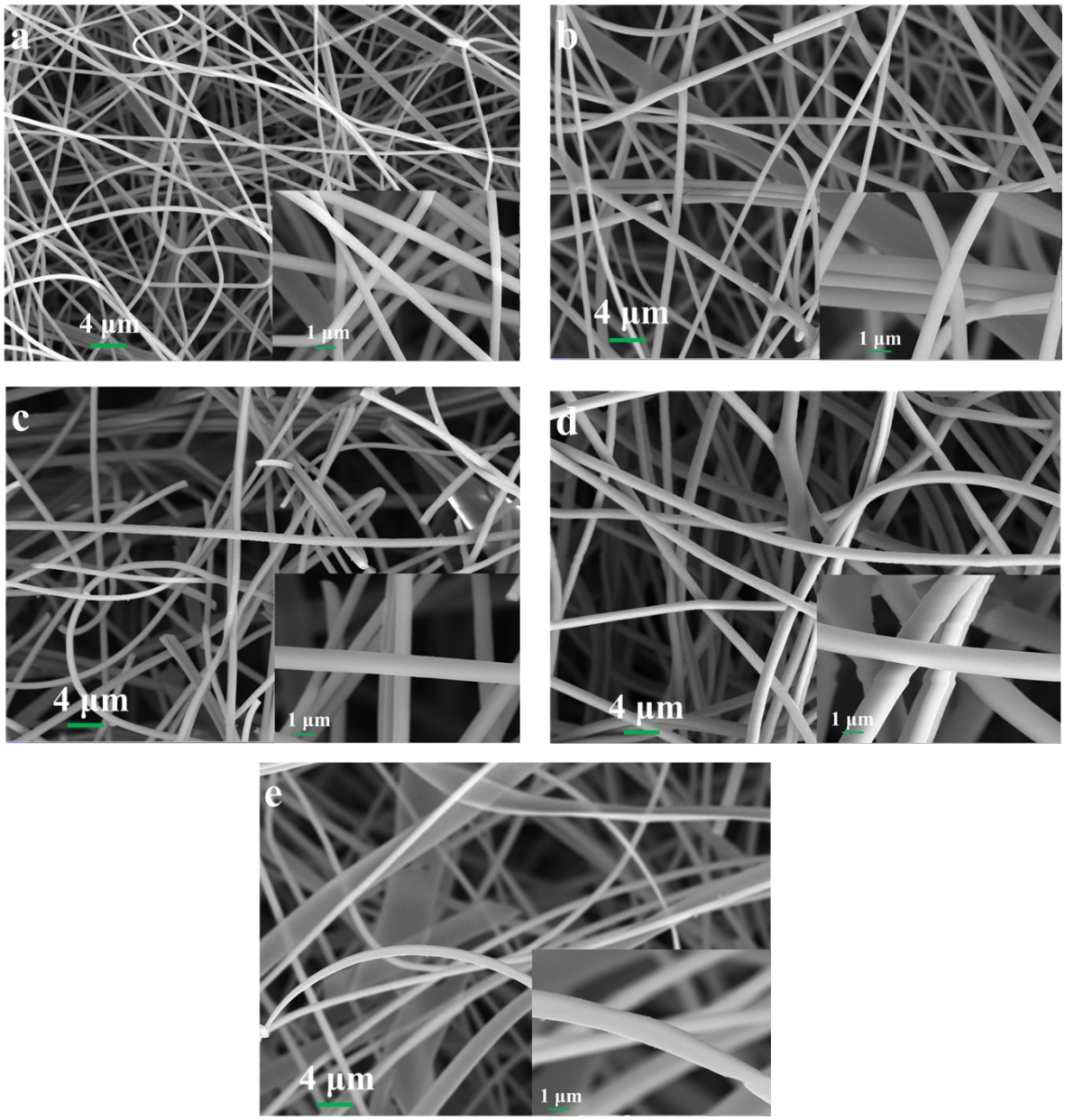

Fig. S8. SEM results of SiO_2 fibrous membranes. (a) Sample 1 ($d_{ave}^{f} = 0.54\mu m$); (b) Sample 2 ($d_{ave}^{f} = 0.80\mu m$); (c) Sample 3 ($d_{ave}^{f} = 0.84\mu m$); (d) Sample 4 ($d_{ave}^{f} = 1.21\mu m$); (e) Sample 5 ($d_{ave}^{f} = 1.32\mu m$).

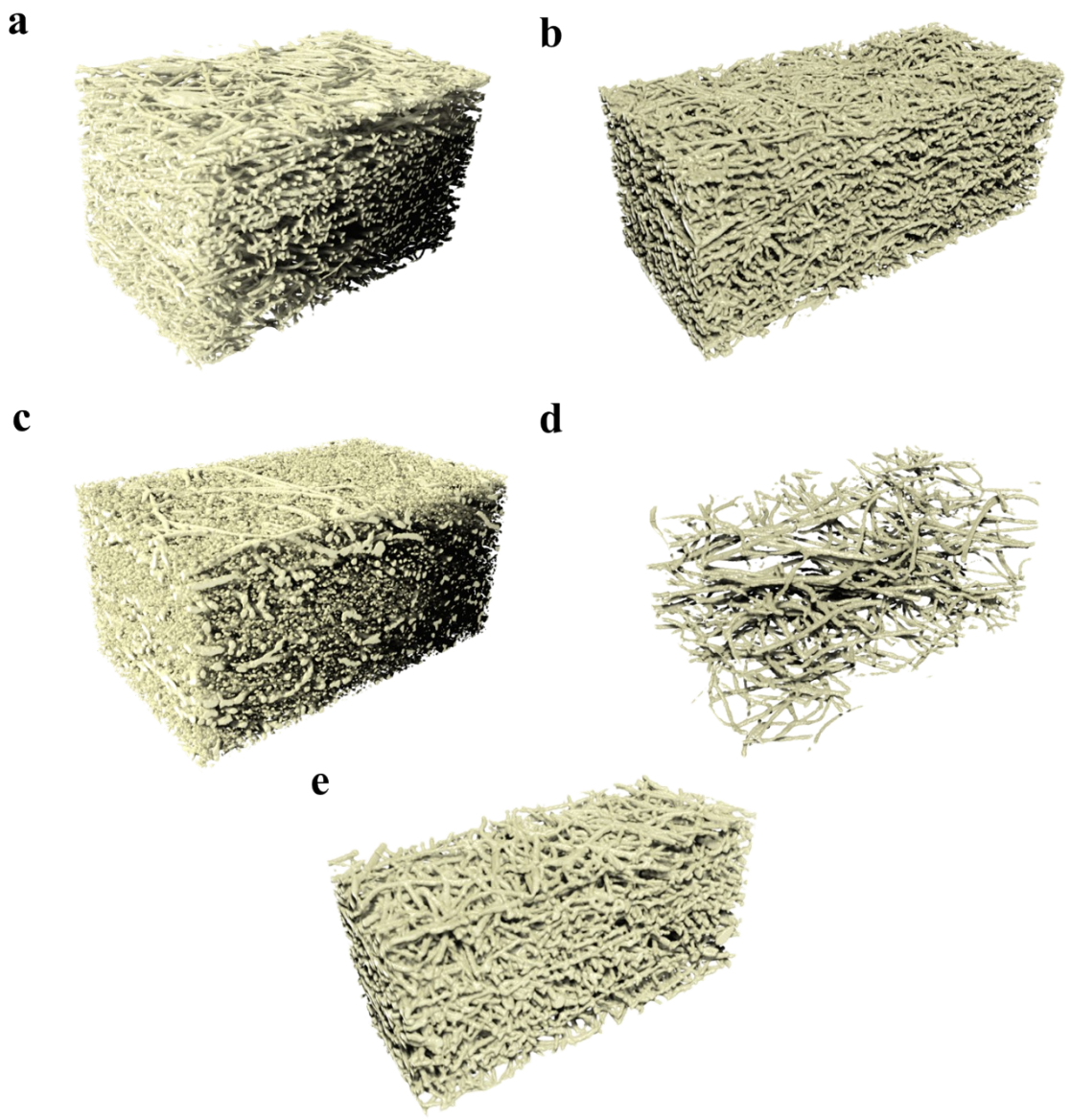

Fig. S9. Reconstruction results of SiO_2 fibrous membranes based on the data of X-ray microimaging. (a) Sample 1 ($\varepsilon = 0.81$); (b) Sample 2 ($\varepsilon = 0.74$); (c) Sample 3 ($\varepsilon = 0.71$); (d) Sample 4 ($\varepsilon = 0.94$); (e) Sample 5 ($\varepsilon = 0.70$).

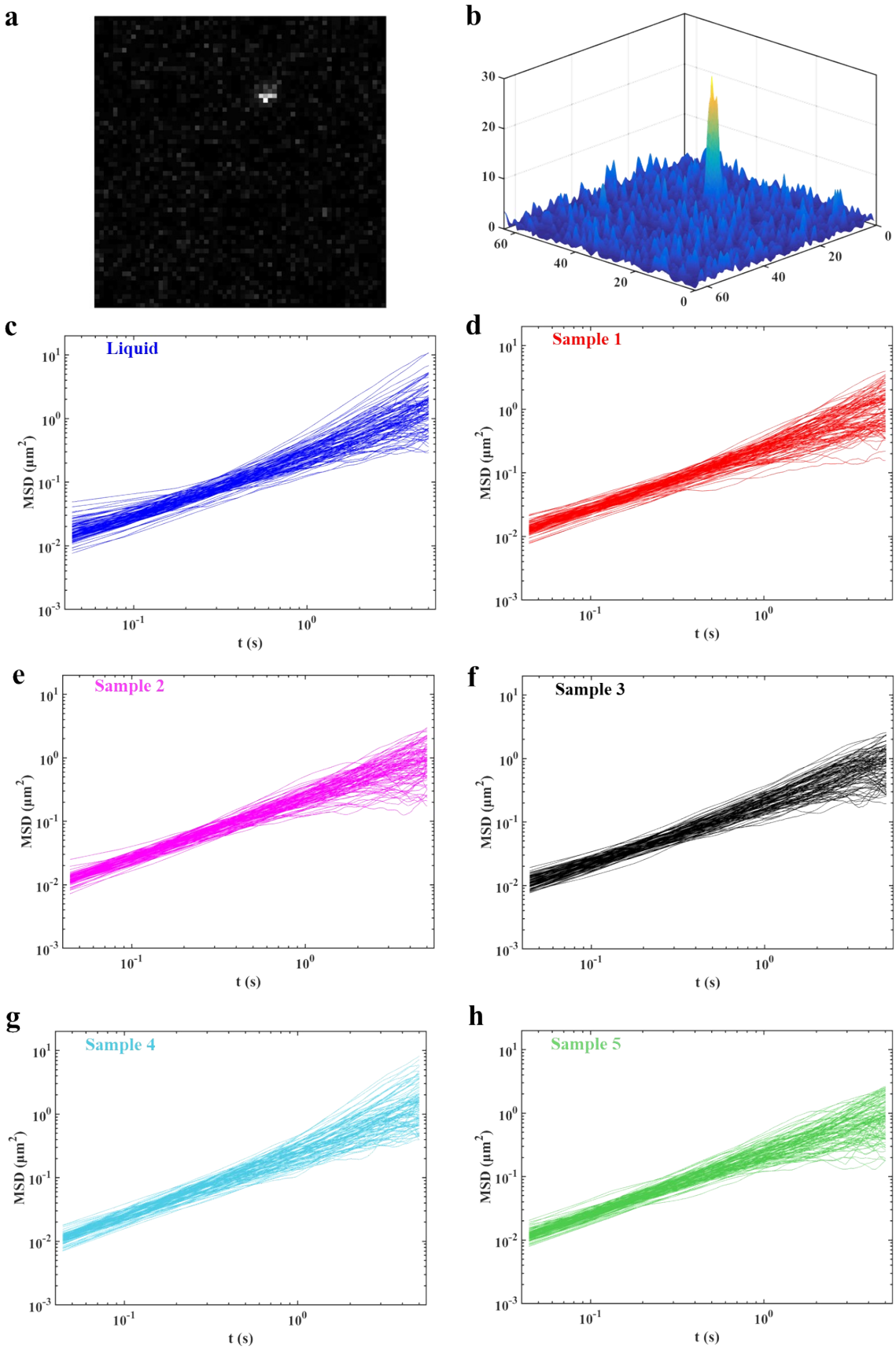

Fig. S10 (a) Raw image of 100 nm NP; (b) Particle grey-scale value distribution. (c-h) Temporally MSD curves for 100 randomly selected nanoparticle trajectories in the (c) liquid, (b-f) sample 1-5.

S3 Validation details for dual-resistance model

Table S3 presents a summary of values used in the errors analysis of the dual resistance model. The D_{eff}/D_0 in Table S3 are obtained by the references from 4 to 13, which were measured by the authors of the references. In Table S3, most of the porous materials are hydrogel polymers with tiny fiber radius (0.5-2 nm). The radius of the polymer is usually estimated by a theoretical formula based on the measured relaxation time of the polymer. Therefore, the radius measured in this way is named by reference fiber radius with limited accuracy.

Table. S3 Summary of the values used in the meta-analysis, including the solute and porous material, polymer volume fraction, experimental diffusivity, solute radius, fitted fiber radius and reference fiber radius

Author(s)	Dimensionless data		Solute material	Porous material	Solute radius r_s (nm)	Fitted fiber radius r_f (nm)	Reference fiber radius (nm)
	1-ε	D_{eff}/D_0					
Kavindya K. Senanayake et al.[4-6]	0.015	0.871	gold nanoparticles	xanthan	2.5	0.3439	1.2
	0.03	0.787					
	0.045	0.693					
	0.075	0.620					
	0.1125	0.459					
	0.1875	0.286					
	0.3	0.225					
	0.45	0.152					
	0.037	0.500		PVA		0.2059	1
	0.072	0.395					
	0.110	0.297					
	0.148	0.229					
	0.077	0.722	Ag nanoparticles	PVA	2.5	0.6373	1
	0.112	0.623					
	0.144	0.598					
	0.174	0.533					
	0.201	0.478					

	0.078	0.658			5	0.919	1
	0.112	0.583					
	0.144	0.539					
	0.174	0.428					
	0.202	0.344					
	0.223	0.242					
G. Majer[7]	0.09	0.576	adenosine triphosphate (ATP)	poly(ethylene glycol) diacrylate (PEG-DA)	0.634	0.9847	NA
	0.18	0.330					
	0.27	0.140					
Zhou et al.[8]	0.05	0.294	LYZ	PSBMA (10 mM)	1.91	0.88	0.996
	0.057	0.228					
	0.065	0.147					
	0.081	0.125					
	0.158	0.015					
	0.05	0.562		PSBMA (150 mM)		1.5	
	0.057	0.530					
	0.065	0.438					
	0.081	0.346					
	0.05	0.618		PSBMA (300 mM)		1.76	
	0.057	0.559					
	0.065	0.519					
	0.081	0.380					
	0.158	0.048					
Nicholas et al.[9]	0.005	0.795	fluorescein dextran (FDX 20)	methacrylated alginate (MALG)	2.8	0.94	0.83
	0.009	0.663					
	0.016	0.518					
	0.022	0.401					
	0.029	0.300					
	0.003	0.886	FDX 10	sodium alginate (ALG)	2	0.90	
	0.006	0.800					
	0.009	0.729					
	0.012	0.672					
	0.003	0.823	FDX 20	ALG	2.8	0.84	
	0.006	0.684					
	0.009	0.600					
	0.012	0.522					
Michael et al.[10]	0.02	0.607	dextran 10 K	agarose	1.7	0.93	1.9
	0.04	0.473					
	0.06	0.322					
	0.02	0.569	dextran 70 K		4.7	2.08	
	0.04	0.278					

	0.06	0.204					
Matsuyama et.al[11]	0.064	0.668	Vit B12	PVA	0.87	1.32	1.2
	0.117	0.504					
	0.138	0.443					
	0.190	0.372					
	0.064	0.318	LYS		1.91	1.30	
	0.117	0.138					
	0.138	0.089					
	0.190	0.019					
Gao et al.[12]	0.008	0.87	adinazolam mesylate (AM)	HPMC	0.54	0.50	NA
	0.016	0.8					
	0.031	0.7					
	0.047	0.6					
	0.063	0.51					
	0.079	0.42					
	0.104	0.35					
	0.119	0.3					
	0.14	0.26					
White et al.[13]	0.046	0.836	Urea	PAAG	0.19	0.61	NA
	0.095	0.806					
	0.175	0.554					
	0.239	0.449					
	0.046	0.739	Glucose		0.48	0.62	
	0.095	0.499					
	0.175	0.259					
	0.239	0.140					

Table S4. Regression results of dual-resistance, steric, and hydrodynamic resistance models versus literature data

Fibrous materials (reference radius, Å)	Solute radius (Å)	Model								
		dual-resistance			Steric			Hydrodynamic		
		r_f fit (Å)	±SE $\times 10^2$	R^2	r_f fit (Å)	±SE $\times 10^2$	R^2	r_f fit (Å)	±SE $\times 10^2$	R^2
PSBMA10 mM[8] (10.0)	LYZ(19.1)	8.8	2.5	0.95	7.11	4.5	0.82	2.5	6.3	0.64
FDX 20 (8.3) [9]	MALG(28)	9.4	2.6	0.98	6.6	9.6	0.77	5.5	8.0	0.84

SE: standard error (95% confidence interval). R: correlation coefficient

References

1. M. H. Blees and J. C. Leyte, *Journal of Colloid and Interface Science*, 1994, **166**, 118-127.
2. B. R. Gebart, *Journal of Composite Materials*, 1992, **26**, 1100-1133.
3. A. Nabovati, E. W. Llewellin and A. C. M. Sousa, *Composites Part A: Applied Science and Manufacturing*, 2009, **40**, 860-869.
4. K. K. Senanayake, E. A. Fakhrabadi, M. W. Liberatore and A. Mukhopadhyay, *Macromolecules*, 2019, **52**, 787-795.
5. K. K. Senanayake and A. Mukhopadhyay, *Langmuir*, 2019, **35**, 7978-7984.
6. K. K. Senanayake, N. Shokeen, E. A. Fakhrabadi, M. W. Liberatore and A. Mukhopadhyay, *Soft Matter*, 2019, **15**, 7616-7622.
7. G. Majer and A. Southan, *J Chem Phys*, 2017, **146**, 225101.
8. Y. Zhou, J. Li, Y. Zhang, D. Dong, E. Zhang, F. Ji, Z. Qin, J. Yang and F. Yao, *J Phys Chem B*, 2017, **121**, 800-814.
9. N. A. Hadjiev and B. G. Amsden, *J Control Release*, 2015, **199**, 10-16.
10. M. B. Albro, V. Rajan, R. Li, C. T. Hung and G. A. Ateshian, *Cell Mol Bioeng*, 2009, **2**, 295-305.
11. H. Matsuyama, M. Teramoto and H. Urano, *Journal of Membrane Science*, 1997, **126**, 151-160.
12. P. Gao and P. E. Fagerness, *Pharm Res*, 1995, **12**, 955-964.
13. M. L. White and G. H. Dorion, *Journal of Polymer Science*, 1961, **55**, 731-740.